Electronic Supplementary Material (ESI) for Chemical Communications.

Benzoquinone-imidazole hybrid organic anolyte for aqueous redox flow battery

Supporting Information

Tsuyoshi Murata,* Marina Hamasaki and Yasushi Morita*

Department of Applied Chemistry, Faculty of Engineering,

Aichi Institute of Technology, Toyota, Aichi 470-0392, Japan.

Experimental section

Materials and Characterization

Tetraamino-*p*-benzoquinone is commercially available (Combi-Blocks/JP-9634 and BLD pharm/BD01317144, etc), and we synthesized according to the literature method from *p*-chloranil.[S1] Other reagents and solvents were used as purchased. Melting and decomposition points were measured with a hot-stage apparatus with a Yanako MP-J3, and were uncorrected. Melting and/or decomposition were detected by eye observation. Elemental analyses were performed at the Graduate School of Science, Osaka University. ^{1}H and ^{13}C NMR spectra of **1** in the solution state were obtained on a JEOL ECA-500 with 1 M KOD in D_2O solution using potassium methanesulfonate (δ = 2.80 ppm) as an internal standard. Infrared spectra were recorded on a Shimadzu Tracer-100 spectrometer using KBr pellets (resolution 4 cm^{-1}). UV-Vis absorption spectra were measured on a Shimadzu UV-3600PC UV/vis scanning spectrophotometer.

Synthesis

Potassium salt of 3,5-dihydroimidazo[4,5-f]benzimidazole-4,8-dione ($K^{+}_{2}\cdot 1^{2-}$). In a 200-mL round-bottomed flask, a mixture of tetraamino-*p*-benzoquinone (2.00 g, 11.9 mmol) and triethyl orthoformate (100 mL, 601 mmol) was stirred at 100 °C for 20 h. After being cooled to room temperature, the excess amount of the reagent was removed by evaporation. The residue was washed with dichloromethane to yield a crude product (2.15 g). The crude product was dissolved in 1 M KOH aqueous solution, and then the insoluble material was removed by filtration. The filtrate was neutralized with 2 M HCl aqueous solution. The precipitate was collected by filtration was washed with water and methanol, to give **1** (1.69 g, 85%) as a dark brown powder.

In a 50-mL flask, **1** (903 mg, 4.80 mmol) was added to 1 M potassium hydroxide solution in ethanol (20 mL). The mixture was stirred at 70 °C for 3 h. The precipitate was collected by filtration was washed with ethanol, to give $\mathbf{K^{+}_{2}\cdot 1^{2-}}$ (1.09 g, 86%) as a grayish brown powder. M.p. >300 °C (in air); ^{1}H NMR (500 MHz, 1 M KOD in D_2O) δ 7.51 (s, 2H) ppm; ^{13}C NMR (500 MHz, 1 M KOD in D_2O) δ 144.67, 150.90, 179.64 ppm; IR (KBr) ν 1699, 1620, 1481, 1458 cm^{-1}; Anal. Calcd for $(C_8H_2N_4O_2K_2)(H_2O)_{2.2}$: C, 31.61; H, 2.12; N, 18.43. Found: C, 31.99; H, 2.06; N, 18.07.

Solubility study

Solubility study of $\mathbf{K^{+}_{2}\cdot 1^{2-}}$ salt was performed using UV/Vis spectroscopy. Calibration curves were obtained by plotting the absorbances against concentration. A saturated solution $\mathbf{K^{+}_{2}\cdot 1^{2-}}$ was obtained by stirring an excess of the solid in 1 M KOH or 1 M KCl aqueous solutions overnight at room temperature. After removing the excess solid by filtration, the saturated solution (100 μL) was diluted to 10 mL of 1 M KOH aqueous solution and then further diluted accordingly to reach the linear range of the calibration curve.

Electrochemical measurements

Electrochemical measurements in the solution state were conducted on an ALS Electrochemical Analyzer model 730A (BAS Co., Ltd., Japan). An Ag/AgCl electrode in 3 M NaCl solution served as reference electrode, a 3 mm-diameter glassy carbon electrode as working electrode, and a Pt wire as counter electrode. Cyclic voltammetry (CV) and linear sweep voltammetry (LSV) measurements were performed at room temperature in 1 M KOH aqueous solution. The redox potentials were finally calibrated with standard hydrogen electrode (SHE). LSV measurement using rotating-disk-electrode (RDE) was carried out using the ALS Electrochemical Analyzer model 730A with RRDE-3A. A glassy carbon rotating disk electrode (3 mm in diameter) was used as the working electrode. Linear sweep voltammetry (LSV) scans were recorded at a scan rate of 10 mV/s.

Kinetics calculation

For Nicholson method (Fig. 2b), the diffusion coefficient (D_0) was calculated by the following formula:

$$i_p = (2.69 \times 10^5)\, n^{3/2}\, A\, D_0^{1/2}\, C_0\, v^{1/2} \qquad \text{(Eq. 1)}$$

i_p: peak current; n: number of electrons involved in the redox process; A: working electrode area; C_0: concentration of active species; D_0: diffusion coefficient; v: scan rate.

By plotting i_p vs. $v^{1/2}$, the diffusion coefficient can be obtained from the gradient of the fitted line

For Koutecký-Levich approach (Fig. 2d and Fig. S3), the diffusion coefficient was calculated according to Levich equation:

$$i_m^{-1} = i_k^{-1} + B_L^{-1}\omega^{-1/2} \qquad \text{(Eq. 2)}$$

$$B_L = 0.620\, n\, F\, A\, C_0\, D^{2/3}\, v^{-1/6} \qquad \text{(Eq. 3)}$$

i_m: measured current; i_k: kinetically-controlled current; ω: rotation speed $\omega = 2\pi\ (N/60)$ rad/s; F: Faraday's constant F = 96485 C/mol; D: diffusion coefficient; v: kinematic viscosity = 0.00942 cm^2/s for 1 M KOH aqueous solution.

By plotting i_m^{-1} vs. $\omega^{-1/2}$ the diffusion coefficient can be calculated from the gradient of the fitted line. The kinetic currents i_k for different overpotentials (η) were obtained from Eq. 2 by drawing the plot of i_m^{-1} vs. $\omega^{-1/2}$ fitting the y intercept. The electron transfer rate constant (k_0) was calculated according to Butler-Volmer equation:

$$\log (i_k) = \log(n\ F\ A\ C_0\ k_0) + \alpha\ n\ F\ \eta\ /\ 2.303\ RT \qquad \text{(Eq. 4)}$$

By plotting $log\ (i_k)$ vs. η, k_0 can be obtained by from the x intercept.

Redox flow battery and measurements

The active electrode area was 2 × 2 cm^2 with serpentine fluidic channels made from graphite. The 280 μm thickness carbon paper (AvCarb, Gas Diffusion Layer MGL280) was used as electrode, and Nafion cation-exchange membrane (NRE-212) was employed as the separator without pretreatment. Galvanostatic measurement of the flow cell was conducted in a N_2-filled glovebox with a TOSCAT-3300K charge-discharge test system (TOYO System Co. Ltd., Japan) at different current densities. The flow rate was 65 mL/min. All tests were conducted at 65 °C.

In the charge/discharge battery test, the cell employed 20 mL of 0.05 M $\mathbf{K^+_2 \cdot 1^{2-}}$ as anolyte and 40 mL of 0.40 M $K_4[Fe(CN)_6]$ with 0.05 M $K_3[Fe(CN)_6]$ as catholyte in 1 M KOH supporting electrolyte. Thus, in order to investigate the performance of only the anolyte $\mathbf{1^{2-}}$, the volume of the catholyte solution was enlarged, and a charge/discharge test was conducted under the condition of a large excess amount of the catholyte. Rate performance test was performed with the current densities of 100 mA/cm^2 to 5 mA/cm^2, then the same cell was used for the cycle performance test. The cycle performance test was demonstrated with the current density of 25 mA/cm^2. The measurements were conducted at 100% SOC.

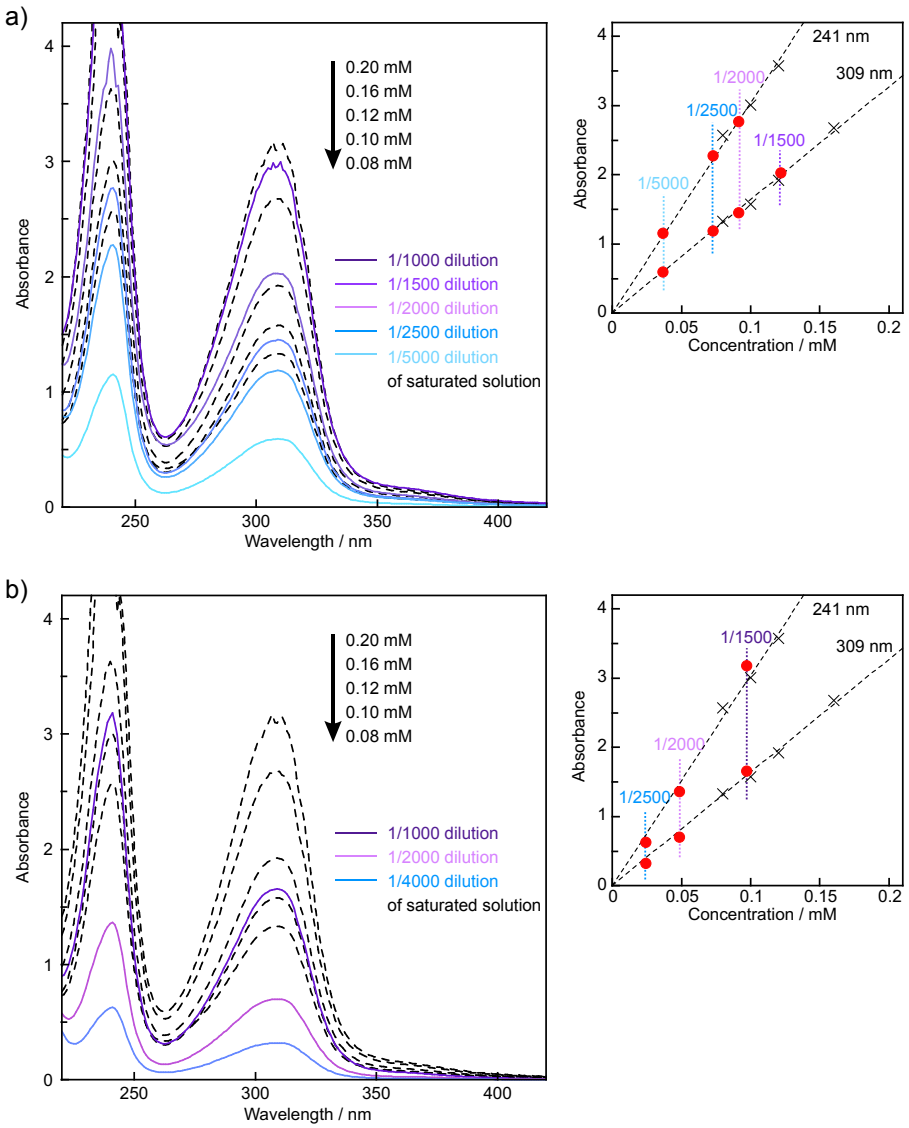

Figure S1. UV/vis absorbance spectra of $\mathbf{K^+_2 \cdot 1^{2-}}$ at different concentrations (dotted lines) and those of diluted samples of the saturated solution in a) 1 M KOH aqueous solution and b) 1 M KCl aqueous solution. The calibration curves from the absorbance spectra are also shown. The molar absorption coefficients for $\mathbf{K^+_2 \cdot 1^{2-}}$ are 1.6×10^4 $M^{-1}cm^{-1}$ at 309 nm and 3.0×10^4 $M^{-1}cm^{-1}$ at 241 nm. The dashed lines in the calibration curves are linear fits to the absorbance vs. concentration data. A baseline of zero absorbance at 550 nm was applied to all spectra.

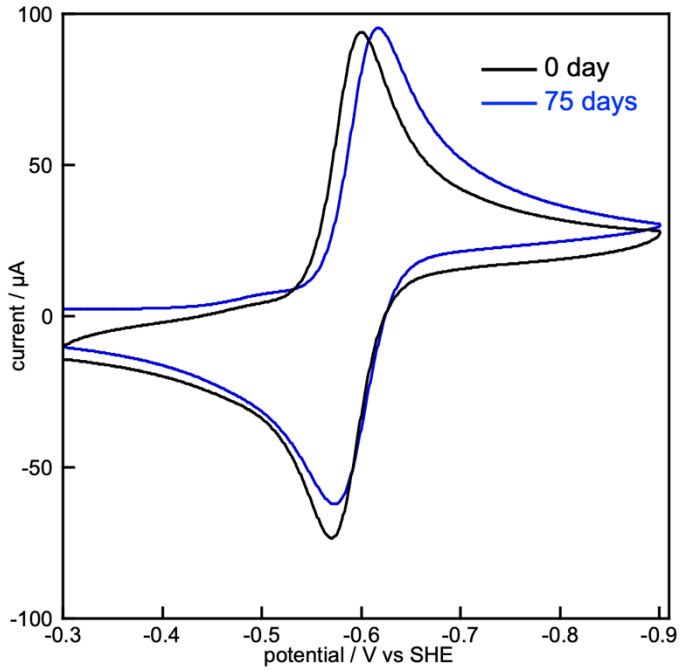

Figure S2. Cyclic voltammetry of $\mathbf{K^{+}_{2}{\cdot}1^{2-}}$ in 1 M KOH aqueous solution using glassy carbon working electrodes, platinum counter electrodes, and Ag/AgCl reference electrodes measured at 25 mV/s. The electrolyte solution was stored for 75 days under air at room temperature.

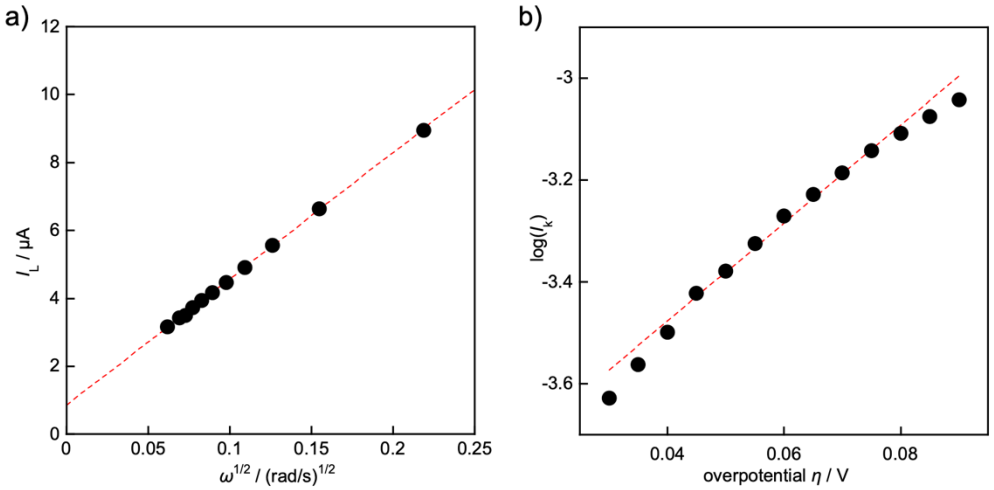

Figure S3. Data analysis for D and k_0 calculations for $\mathbf{1}^{2-}$ from the LSV measurement in 1 M KOH aqueous solution on a glassy carbon RDE (0.07 cm^2) at a scan rate of 10 mV s^{-1} (Fig. 2c). a) Levich plot (I_L vs. $\omega^{1/2}$) for the calculation of D. b) Koutecký-Levich plot (log(I_k) vs. η) for the calculation of k_0.

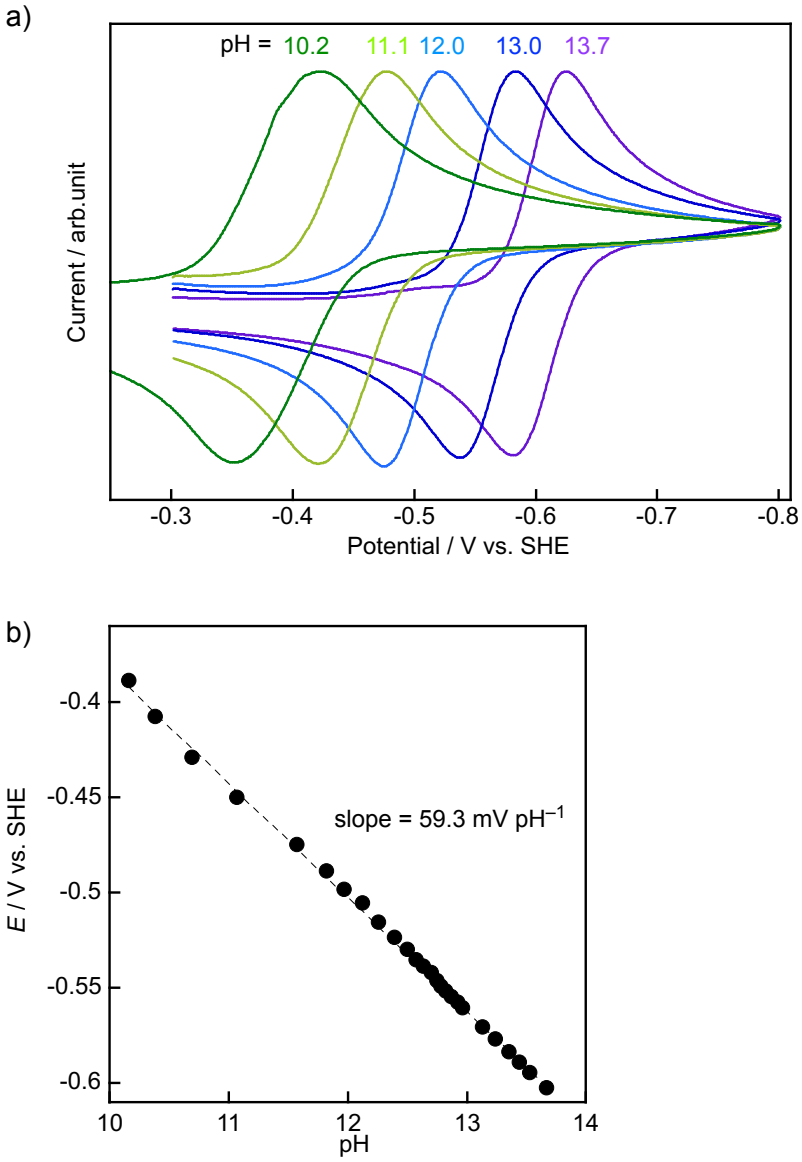

Figure S4. a) Cyclic voltammetry of $\mathbf{K^{+}_{2}{\cdot}1^{2-}}$ at different pH values. The measurement was performed by titrating a 1 M HCl aqueous solution into a 5 mM solution of $\mathbf{K^{+}_{2}{\cdot}1^{2-}}$ in 1 M KOH aqueous solution. The curves are normalized by the peak currents of the reduction waves. Solid precipitation was observed at pH 10.1. b) The Pourbaix diagram calculated from the CV curves measured at different pH values.

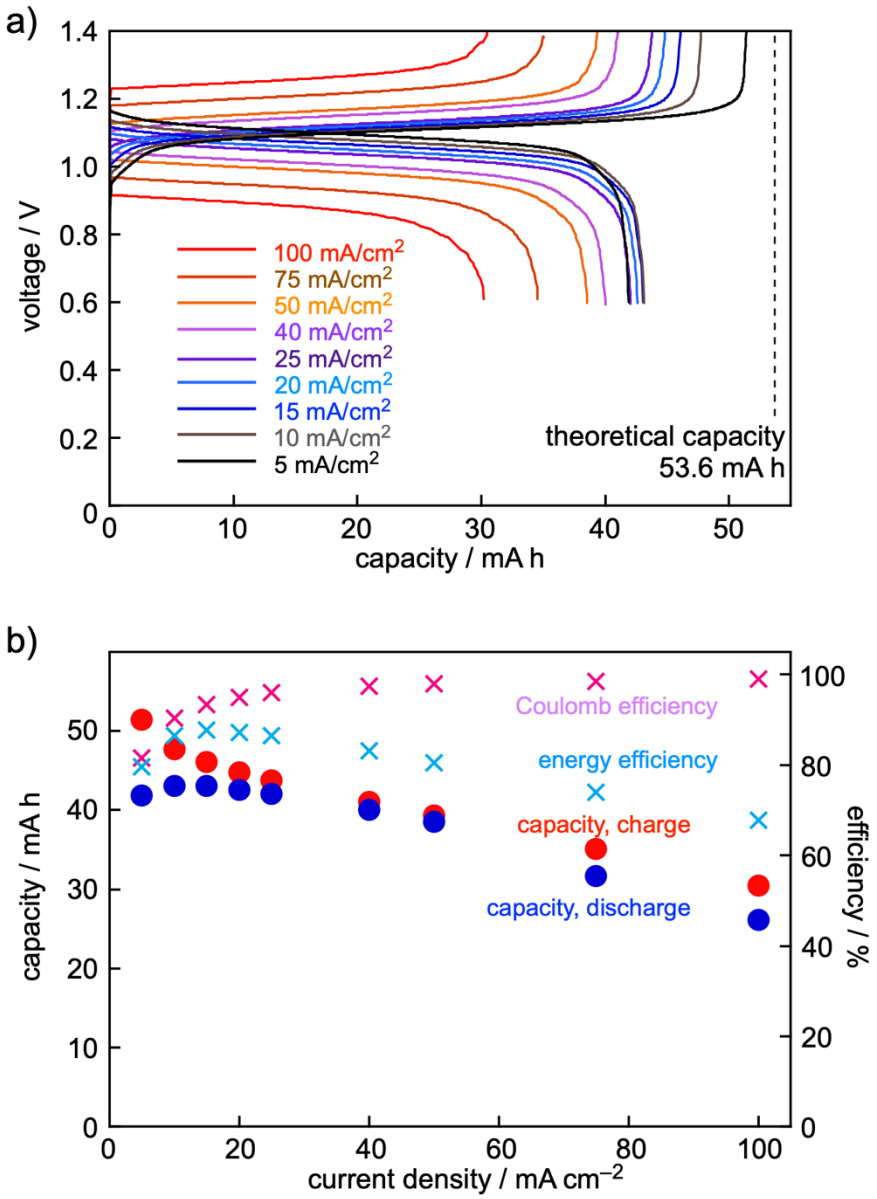

Figure S5. a) Rate performance of 0.05 M $\mathbf{K^{+}_{2}{\cdot}1^{2-}}$ (40 mL)/0.4 M $K_4[Fe(CN)_6]$ + 0.05 M $K_3[Fe(CN)_6]$ (40 mL) flow cell in 1 M KOH aqueous solution. Current densities were tested between 100 and 5 mA cm^{-2}. Voltage limits of 1.4 V and 0.4 V were applied for the experiment. b) Plot of charge/discharge capacities, Coulomb efficiency, energy efficiency, with the current densities in (a).

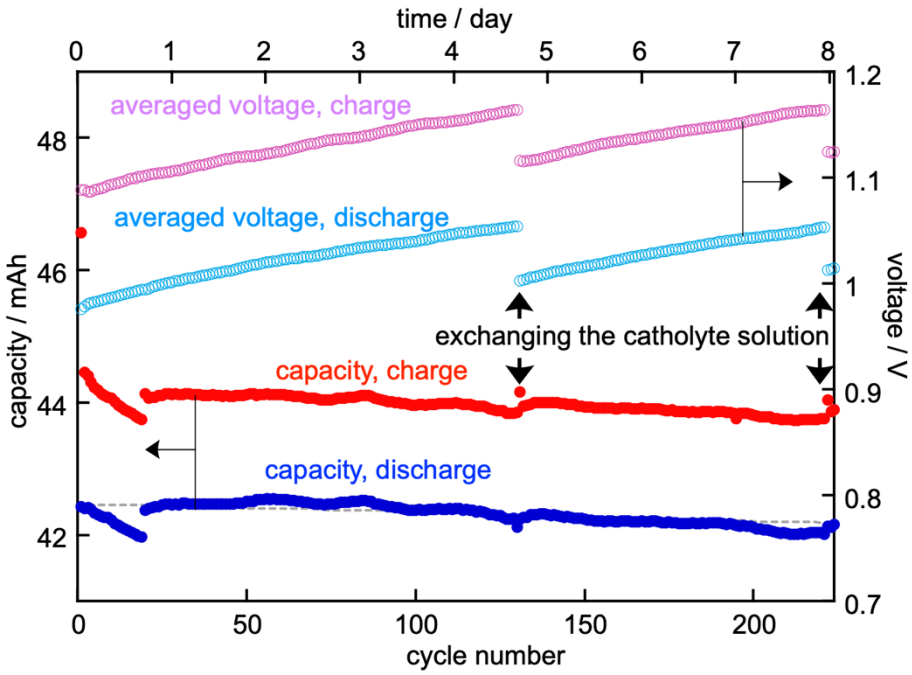

Figure S6. Plots of cycle number vs. charge/discharge capacity and voltage at a current density of 25 mA cm^{-2} in the RFB test of $\mathbf{K^{+}_{2}{\cdot}1^{2-}}$ in a 1 M KOH aqueous solution. Probably due to decomposition of the cathode active material ($K_3[Fe(CN)_6]$) in the strong alkaline aqueous solution or some changes in the electrolyte, the cell voltage gradually increased with repeating charge/discharge cycles. In addition, the capacity also decreased slightly. However, when the catholyte solution was replaced to a flesh one, both the voltage and the capacity returned to their initial values. The capacity fade rate of the anolyte was calculated from the discharge capacities of the cycles in which the capacity became stable after exchanging the catholyte solution (22th, 135th, 224th cycles, gray dotted line).

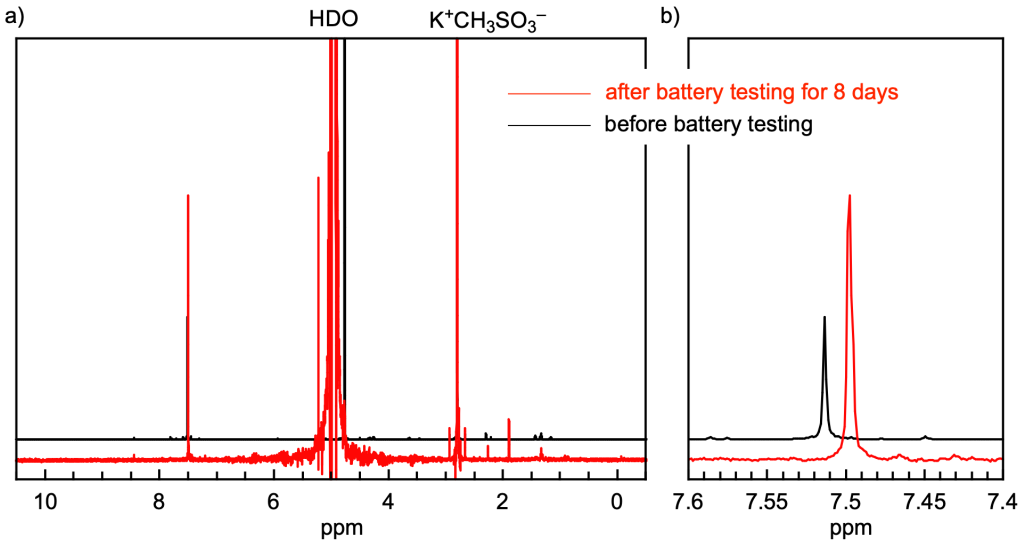

Figure S7. ^{1}H NMR spectrum of $\mathbf{1}^{2-}$ anolyte before and after battery cycling. a) The entire area of the measurement range, and b) the expanded area of the aromatic region. After the cycle performance test, 100 µL of the anolyte solution was diluted with 900 µL of degassed 1 M KOD solution in D_2O. This solution was placed in an NMR tube (Wilmad® low pressure/vacuum NMR tube) in a glove box, sealed, and immediately subjected to the ^{1}H NMR measurement. The chemical shifts were calibrated with potassium methanesulfonate (δ = 2.80 ppm) as an internal standard. The difference of the chemical shift and signal intensity of the signal around 7.5 ppm assignable to $\mathbf{1}^{2-}$ are probably caused by the changes in pH and ion concentration in the anolyte solution during the charge/discharge cycles.

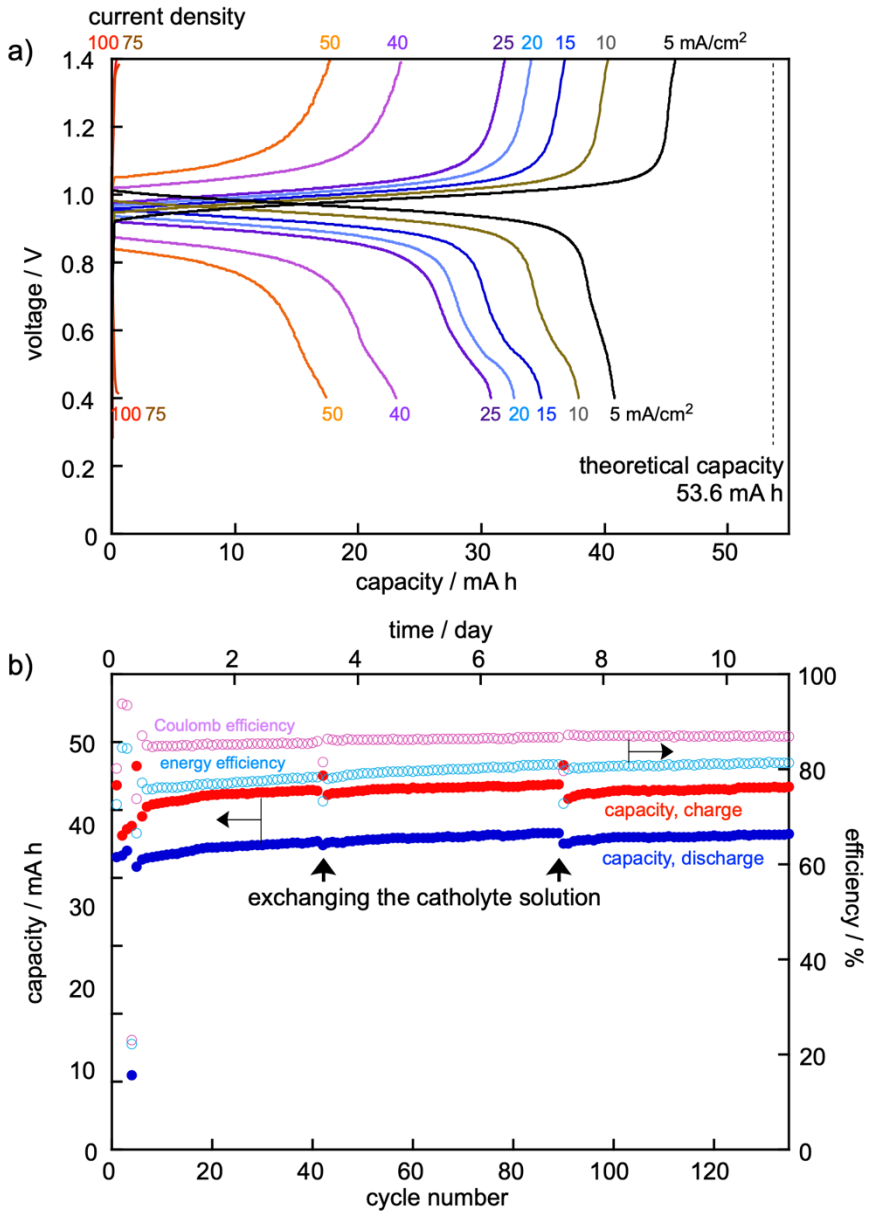

Figure S8. a) Rate performance of 0.025 M $\mathbf{K^{+}_{2}{\cdot}1^{2-}}$ (40 mL)/0.4 M $K_4[Fe(CN)_6]$ + 0.05 M $K_3[Fe(CN)_6]$ (40 mL) flow cell in 1 M KCl aqueous solution. Voltage limits of 1.4 V and 0.4 V were applied for the experiment. b) Cycling performance of the flow cell, where the current density was 10 mA cm^{-2}. The cell was tested in a N_2-filled glove box. The capacity increased slightly with repeating charge/discharge cycles (~8% over 11 days). The reason of this behavior is not clear, however since the pH value of the anolyte solution increased to 14 after the 11 days cycles, some changes such as the ion concentration in the electrolyte may be related.

Table S1. Comparison of some reported aqueous RFBs utilizing organic anolytes and $Fe[(CN)_6]^{4-}/Fe[(CN)_6]^{3-}$ catholyte.

anolyte	solubility	test conditions	$E_{1/2}$ (V vs. SHE) /E_{cell}	cycles, capacity fading rate	volumetric capacity	Ref.
$K^+_2 \cdot 1^{2-}$	0.18 M in 1 M KOH aq	0.05 M in 1 M KOH aq pH 14*	–0.60 V /1.08 V	224 cycles 0.0030%/cycle; 0.081%/day	2.1 mA h/cm^3	This work
$K^+_2 \cdot 1^{2-}$	0.10 M in 1 M KCl aq	0.025 M in 1 M KCl aq pH 11.2	–0.60 V /0.95 V	135 cycles slightly increased	0.95 mA h/cm^3	This work
2,3-HCNQ	1.2 M in 1 M KOH aq	0.5 M in 2 M KOH aq pH 14*	–0.53 V /1.02 V	100 cycles 0.011%/cycle; 3.4%/day	18.8 mA h/cm^3	S2
DHBQ	4.31 M in 1 M KOH aq	0.5 M in 2 M KOH aq pH 14*	–0.72 V /1.21 V	150 cycles 0.24%/cycle; 9%/day	23.2 mA h/cm^3	S3
2,6-DHAQ	>0.6 M in 1 M KOH aq	0.5 M in 2 M KOH aq pH 14*	–0.70 V /1.2 V	100 cycles 0.1%/cycle; 8%/day	26.8 mA h/cm^3 (theoretical)	S4
PEGAQ	2.24 M in 1 M KCl aq	1.5 M in 1 M KCl aq pH 7*	–0.43 V /1.0 V	220 cycles 0.043%/cycle; 0.5%/day	80.4 mA h/cm^3	S5
2,6-DBEAQ	1.1 M in 1 M KOH aq	0.5 M in 0.01 M KOH aq, pH 12*	–0.52 V /1.05 V	250 cycles 0.001%/cycle; 0.05%/day	22.9 mA h/cm^3	S6
2,6-N-TSAQ	0.4 M in 1 M NaOH aq	0.1 M in 1 M NaOH aq pH 14*	–0.62 V /1.14 V	800 cycles 0.00024%/cycle; 0.025%/day	4.76 mA h/cm^3	S7
2,6-DPPEAQ	0.75 M in pH 9 KOH aq (K_4^+ salt)	0.5 M in pH 9 KOH aq (K_4^+ salt)	–0.47 V /1.0 V	480 cycles 0.00036%/cycle; 0.014%/day	24.7 mA h/cm^3	S8
R-Vi	1.1 M in 1 M KCl aq	0.5 M in 1 M KCl aq pH 7*	–0.55 V /1.05 V	3200 cycles 0.021%/cycle; 1.11%/day	11.1 mA h/cm^3	S9
BPPV	1.23 M	1.0 M in NH_4OH aq pH 9	–0.46 V /0.9 V	500 cycles 0.00069%/cycle; 0.016%/day	26.6 mA h/cm^3	S10
ACA	2 M in 1 M KOH aq	1 M in 4 M KOH aq, pH 14*	–0.65 V /1.2 V	400 cycles 0.013%/cycle; 1.2%/day	54 mA h/cm^3 (theoretical)	S11
FMN-Na	>1.5 M in 1 M KOH aq with 3 M nicotinamide	0.24 M in 1 M KOH aq with 1 M nicotinamide pH 14*	–0.517 V /1.1 V	200 cycles 0.02%/cycle; 0.68%/day	5.03 mA h/cm^3	S12
1,6-DPAP	1 M in H_2O	0.5 M in 1 M KCl aq pH 8	–0.56 V /1.15 V	350 cycles 0.000002%/cycle; 0.0015%/day	~23 mA h/cm^3	S13
1,8-PFP	1.46 M in 1 M KOH aq	1.0 M in 1 M KOH aq pH 14*	–0.588 V /1.15 V	400 cycles ~0%/cycle; ~0%/day	50.6 mA h/cm^3	S14
DHPS	1.8 M in 1 M KOH aq	1.4 M in 1 M NaOH aq pH 14*	–0.86 V/ 1.45 V	1400 cycles 0.0195%/cycle; 0.68%/day	67 mA h/cm^3	S15
BHPC	1.55 M in 1 M KOH aq	0.5 M in 1 M KOH aq pH 14*	–0.78 V/ 1.38 V	1300 cycles 0.0015%/cycle; 0.08%/day	25.9 mA h/cm^3	S16

*The pH values are speculated from the alkaline concentration of the electrolyte.

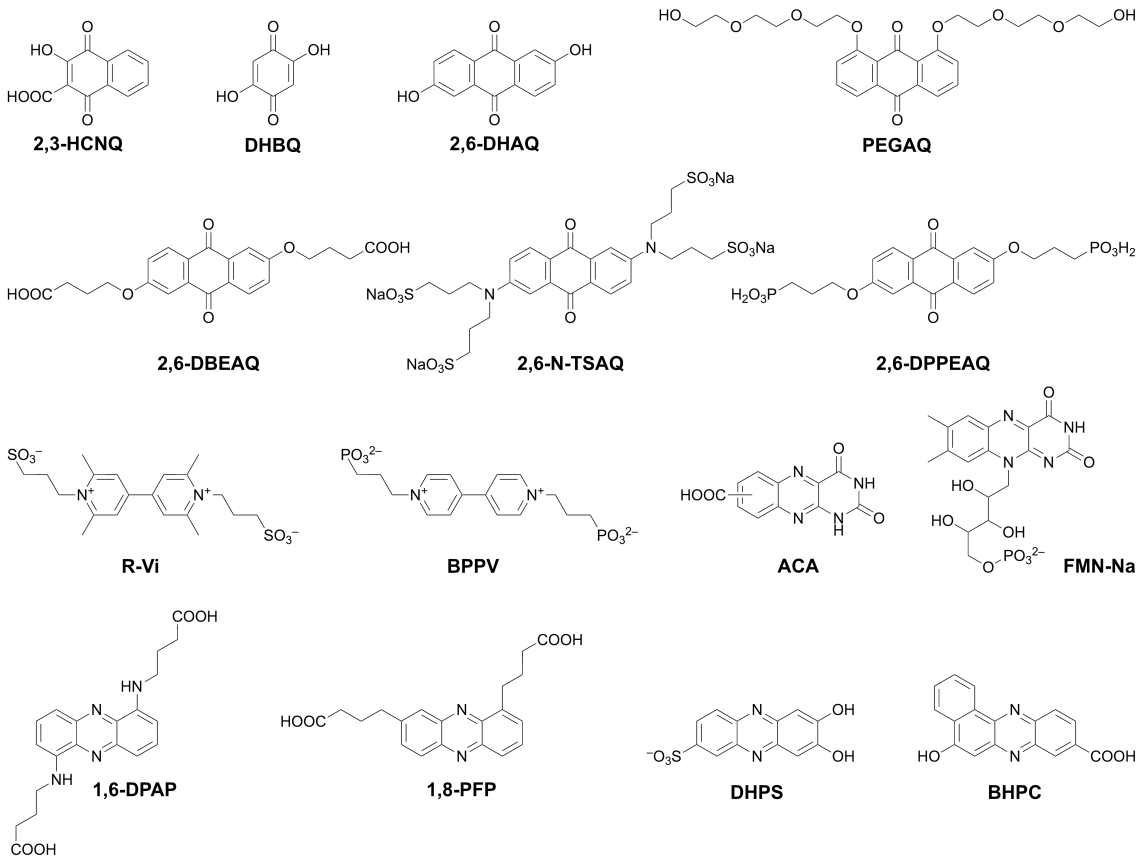

Figure S8. Chemical structures of the anolytes in Table S1.

references

S1 Z. Luo, L. Liu, J. Ning, K. Lei, Y. Lu, F. Li and J. Chen, *Angew. Chem. Int. Ed.*, 2018, **57**, 9443.

S2 C. X. Wang, Z. Yang, Y. R. Wang, P. Y. Zhao, W. Yan, G. Y. Zhu, L. B. Ma, B. Yu, L. Wang, G. G. Li, J. Liu and Z. Jin, *ACS Energy Lett.*, 2018, **3**, 2404.

S3 Z. Yang, L. Tong, D. P. Tabor, E. S. Beh, M.-A. Goulet, D. De Porcellinis, A. Aspuru-Guzik, R. G. Gordon and M. J. Aziz, *Adv. Energy Mater.*, 2018, **8**, 1702056.

S4 K. X. Lin, Q. Chen, M. R. Gerhardt, L. C. Tong, S. B. Kim, L. Eisenach, A. W. Valle, D. Hardee, R. G. Gordon, M. J. Aziz and M. P. Marshak, *Science*, 2015, **349**, 1529.

S5 S. J. Jin, Y. Jing, D. G. Kwabi, Y. L. Ji, L. C. Tong, D. De Porcellinis, M. A. Goulet, D. A. Pollack, R. G. Gordon and M. J. Aziz, *ACS Energy Lett.*, 2019, **4**, 1342.

S6 D. G. Kwabi, K. Lin, Y. Ji, E. F. Kerr, M.-A. Goulet, D. De Porcellinis, D. P. Tabor, D. A. Pollack, A. Aspuru-Guzik, R. G. Gordon and M. J. Aziz, *Joule*, 2018, **2**, 1894.

S7 M. Wu, M. Bahari, Y. Jing, K. Amini, E. M. Fell, T. Y. George, R. G. Gordon and M. J. Aziz, *Batteries & Supercaps* 2022, **5**, e202200009.

S8 Y. L. Ji, M.-A. Goulet, D. A. Pollack, D. G. Kwabi, S. J. Jin, D. D. Porcellinis, E. F. Kerr, R. G. Gordon and M. J. Aziz, *Adv. Energy Mater.*, 2019, **9**, 1900039.

S9 H. B. Li, H. Fan, B. Hu, L. L. Hu, G. Chang and J. X. Song, *Angew. Chem., Int. Ed.*, 2021, **60**, 26971.

S10 J. S. Jin, E. M. Fell, L. Vina-Lopez, Y. Jing, P. W. Michalak, R. G. Gordon and M. J. Aziz, *Adv. Energy Mater.*, 2020, **10**, 2000100.

S11 K. Lin, R. Gómez-Bombarelli, E. S. Beh, L. Tong, Q. Chen, A. Valle, A. Aspuru-Guzik, M. J. Aziz and R. G. Gordon, *Nat. Energy*, 2016, **1**, 16102.

S12 A. Orita, M. G. Verde, M. Sakai and Y. S. Meng, *Nat. Commun.*, 2016, **7**, 13230.

S13 S. Pang, X. Y. Wang, P. Wang and Y. L. Ji, *Angew. Chem., Int. Ed.*, 2021, **60**, 5289.

S14 J. C. Xu, S. Pang, X. Y. Wang, P. Wang and Y. L. Ji, *Joule*, 2021, **5**, 2437.

S15 A. Hollas, X. L. Wei, V. Murugesan, Z. M. Nie, B. Li, D. Reed, J. Liu, V. Sprenkle and W. Wang, *Nat. Energy*, 2018, **3**, 508.

S16 C. X. Wang, X. Li, B. Yu, Y. R. Wang, Z. Yang, H. Z. Wang, H. Lin, J. Ma, G. G. Li and Z. Jin, *ACS Energy Lett.*, 2020, **5**, 411.